HHS Public Access

Author manuscript

*Neuroimage*. Author manuscript; available in PMC 2022 December 23.

Published in final edited form as:

*Neuroimage*. 2022 November 15; 262: 119584. doi:10.1016/j.neuroimage.2022.119584.

# Thalamic nuclei atrophy at high and heterogenous rates during cognitively unimpaired human aging

**Eun Young Choi**[a], **Lu Tian**[b], **Jason H. Su**[c,d], **Matthew T. Radovan**[e], **Thomas Tourdias**[f,g], **Tammy T. Tran**[h], **Alexandra N. Trelle**[h], **Elizabeth Mormino**[i,j], **Anthony D. Wagner**[h,j], **Brian K. Rutt**[c,j,*]

[a]Department of Neurosurgery, Stanford University, 300 Pasteur Drive, MC5327, Stanford, CA 94305, USA

[b]Department of Biomedical Data Science, 1265 Welch Road, MC5464, Stanford, CA 94305, USA

[c]Department of Radiology, Stanford University, 300 Pasteur Drive, MC5488, Stanford, CA 94305, USA

[d]Department of Electrical Engineering, Stanford University, 350 Jane Stanford Way, MC9505, Stanford, CA 94305, USA

[e]Department of Computer Science, Stanford University, 353 Jane Stanford Way, MC9025, Stanford, CA 94305, USA

[f]Department of Neuroradiology, Bordeaux University Hospital, Bordeaux, France

[g]INSERM U1215, Neurocentre Magendie, University of Bordeaux, France

[h]Department of Psychology, Stanford University, Building 420, MC2130, Stanford, CA 94305, USA

[i]Department of Neurology and Neurological Sciences, Stanford, University, 300 Pasteur Drive, MC5235, Stanford, CA 94305, USA

[j]Wu Tsai Neurosciences Institute, Stanford University, 290 Jane Stanford Way, Stanford, CA 94305, USA

## Abstract



*Corresponding author. brutt@stanford.edu (B.K. Rutt).

Declaration of Competing Interest

None

Credit authorship contribution statement

**Eun Young Choi:** Conceptualization, Methodology, Software, Investigation, Data curation, Writing – original draft, Visualization. **Lu Tian:** Formal analysis, Writing – review & editing. **Jason H. Su:** Conceptualization, Methodology, Software. **Matthew T. Radovan:** Methodology, Software. **Thomas Tourdias:** Methodology, Resources, Investigation, Writing – review & editing. **Tammy T. Tran:** Methodology, Resources, Investigation, Writing – review & editing. **Alexandra N. Trelle:** Methodology, Resources, Writing – review & editing. **Elizabeth Mormino:** Methodology, Resources, Writing – review & editing. **Anthony D. Wagner:** Methodology, Resources, Writing – review & editing. **Brian K. Rutt:** Conceptualization, Methodology, Software, Formal analysis, Data curation, Writing – original draft, Visualization, Supervision, Project administration, Funding acquisition.

Supplementary materials

Supplementary material associated with this article can be found, in the online version, at doi:10.1016/j.neuroimage.2022.119584.

The thalamus is a central integration structure in the brain, receiving and distributing information among the cerebral cortex, subcortical structures, and the peripheral nervous system. Prior studies clearly show that the thalamus atrophies in cognitively unimpaired aging. However, the thalamus is comprised of multiple nuclei involved in a wide range of functions, and the age-related atrophy of individual thalamic nuclei remains unknown. Using a recently developed automated method of identifying thalamic nuclei (3T or 7T MRI with white-matter-nulled MPRAGE contrast and THOMAS segmentation) and a cross-sectional design, we evaluated the age-related atrophy rate for 10 thalamic nuclei (AV, CM, VA, VLA, VLP, VPL, pulvinar, LGN, MGN, MD) and an epithalamic nucleus (habenula). We also used T1-weighted images with the FreeSurfer SAMSEG segmentation method to identify and measure age-related atrophy for 11 extra-thalamic structures (cerebral cortex, cerebral white matter, cerebellar cortex, cerebellar white matter, amygdala, hippocampus, caudate, putamen, nucleus accumbens, pallidum, and lateral ventricle). In 198 cognitively unimpaired participants with ages spanning 20–88 years, we found that the whole thalamus atrophied at a rate of 0.45% per year, and that thalamic nuclei had widely varying age-related atrophy rates, ranging from 0.06% to 1.18% per year. A functional grouping analysis revealed that the thalamic nuclei involved in cognitive (AV, MD; 0.53% atrophy per year), visual (LGN, pulvinar; 0.62% atrophy per year), and auditory/vestibular (MGN; 0.64% atrophy per year) functions atrophied at significantly higher rates than those involved in motor (VA, VLA, VLP, and CM; 0.37% atrophy per year) and somatosensory (VPL; 0.32% atrophy per year) functions. A proximity-to-CSF analysis showed that the group of thalamic nuclei situated immediately adjacent to CSF atrophied at a significantly greater atrophy rate (0.59% atrophy per year) than that of the group of nuclei located farther from CSF (0.36% atrophy per year), supporting a growing hypothesis that CSF-mediated factors contribute to neurodegeneration. We did not find any significant hemispheric differences in these rates of change for thalamic nuclei. Only the CM thalamic nucleus showed a sex-specific difference in atrophy rates, atrophying at a greater rate in male versus female participants. Roughly half of the thalamic nuclei showed greater atrophy than all extra-thalamic structures examined (0% to 0.54% per year). These results show the value of white-matter-nulled MPRAGE imaging and THOMAS segmentation for measuring distinct thalamic nuclei and for characterizing the high and heterogeneous atrophy rates of the thalamus and its nuclei across the adult lifespan. Collectively, these methods and results advance our understanding of the role of thalamic substructures in neurocognitive and disease-related changes that occur with aging.

### Keywords

Thalamus; Thalamic nuclei; Atrophy; Cognitively unimpaired aging; White matter nulled imaging; THOMAS segmentation

## 1. Introduction

Atrophy of brain tissue is a classic hallmark of aging. Brain atrophy reflects the shrinkage and loss of neurons and the connections between them (Fjell and Walhovd, 2010). While brain atrophy is a prominent feature in many brain diseases, atrophy can also be seen both broadly and focally in the cognitively unimpaired aging brain (Fjell and Walhovd, 2010). Characterizing brain structural changes during cognitively unimpaired aging will

inform efforts to understand the differences between normal and disease-related atrophy, the structural changes that can be tolerated before they significantly impact function, and the resiliency of the cognitively unimpaired aging brain.

Within the brain, the thalamus is a central integration structure, receiving and distributing information among the cerebral cortex, subcortical structures, and the peripheral nervous system via the brainstem (Steriade et al., 1997). This high degree of integration is accomplished in part by thalamic projection neurons that send long-range outputs with collateral projections and large ramifications at their targets (Steriade et al., 1997). This processing is organized by intra-thalamic nuclei dedicated to distinct functions, including cognitive, visual, auditory, vestibular, and sensorimotor functions (Steriade et al., 1997). Lesions of thalamic nuclei lead to profound disruptions in the modulation of behaviors subserved by these functional domains (Carrera and Bogousslavsky, 2006). As a highly connected and integrative structure in the brain, the thalamus is in a critical but also vulnerable position that may show prominent structural changes resulting from age-related changes across the brain, such as degeneration due to reduced connectivity or accumulated oxidative stress from high levels of neuronal activity.

Current knowledge of age-related thalamic volumetric changes in humans comes primarily from neuroimaging studies which show that the thalamus as a whole significantly atrophies over the cognitively unimpaired adult lifespan (Cherubini et al., 2009; Fjell et al., 2013; Goodro et al., 2012; Hughes et al., 2012; Long et al., 2012; Murphy et al., 1996, 1993; Narvacan et al., 2017; Nyberg et al., 2010; Raji et al., 2009; Schippling et al., 2017; Squarzoni et al., 2018; Su et al., 2012; Takahashi et al., 2011; Tullo et al., 2019; Van Der Werf et al., 2001; Walhovd et al., 2005, 2011; Yoo et al., 2016; Zheng et al., 2019). Postmortem histological studies afford a higher resolution characterization of the volumes of thalamic nuclei. However, while there are a number of postmortem human histological studies showing that thalamic nuclear volumes and neuronal counts are reduced in disease (Byne et al., 2002; Popken et al., 2000; Young et al., 2000), to our knowledge, there are no such studies of cognitively unimpaired human aging. Thus, as yet, we do not know the rates of volumetric change of specific thalamic nuclei over the cognitively unimpaired adult lifespan (Fama and Sullivan, 2015). Such studies would identify whether age-related neurodegeneration is occurring heterogeneously within the thalamus, and therefore whether the concept of “regional vulnerability” (Small, 2014) applies to the thalamus.

Recently, our group developed an automated image segmentation method that non-invasively and accurately identifies 10 thalamic nuclei and two adjacent structures. This method uses 3T or 7T MRI with white-matter-nulled magnetization prepared rapid acquisition gradient echo (WMnMPRAGE) contrast, which provides higher contrast in the thalamus than conventional MPRAGE imaging in which the cerebrospinal fluid (CSF) is nulled (Saranathan et al., 2015; Tourdias et al., 2014). WMnMPRAGE image contrast is strong enough to manually identify individual thalamic nuclei and adjacent structures (Tourdias et al., 2014). Our automated thalamic segmentation method, known as THOMAS (THalamus Optimized Multi-Atlas Segmentation), was trained using manual delineations of these identifiable structures in a set of 20 training volumes to create a multi-atlas label-fusion segmentation tool that accurately identifies 10 thalamic nuclei and two adjacent structures

(Su et al., 2019). THOMAS has been used to characterize the volumes of thalamic nuclei in cognitively unimpaired versus patient populations of multiple sclerosis (Planche et al., 2020), alcoholism and HIV (Zahr et al., 2020), and essential tremor (Su et al., 2020).

In the present study, our principal goal was to characterize the structural changes of thalamic nuclei over the adult lifespan in cognitively unimpaired participants using a cross-sectional approach. This was done by applying THOMAS to segment thalamic nuclei within WMnMPRAGE image volumes acquired from a large group of 198 cognitively unimpaired adult participants with ages ranging from 20 to 88 years. Our secondary goal was to compare the atrophy of thalamic nuclei with those of extra-thalamic regions, with the latter segmented using conventional T1-weighted images of the same participants and the Sequence Adaptive Multimodal SEGmentation (SAMSEG) tool within the FreeSurfer suite of neuroimaging analysis tools. We employed an exponential regression model to estimate atrophy rates (annualized percent change in volume) and differences in atrophy rates among thalamic nuclei and extra-thalamic structures.

## 2. Material and methods

### 2.1. Participants

198 Cognitively unimpaired adult participants (86 M, 112 F) were recruited, with a mean age of 59.4 years and an age range of 20 to 88 years at the time of imaging (Table 1). Older participants (>=60 years of age, $n$ = 143, 66 M, 77 F) were recruited at Stanford University as part of the Stanford Aging and Memory Study (SAMS) (Trelle et al., 2020, 2021). Younger participants (<60 years of age) were recruited at Stanford University ($n$ = 17, 9 M, 8 F) and at the University of Bordeaux ($n$ = 38, 11 M, 27 F). Written informed consent was obtained for all participants and study procedures were approved by each institution's Institutional Review Board. Participants were screened against neurological and psychiatric disease. Older participants were additionally screened to have a Clinical Dementia Rating (CDR) (Morris, 1993) score of zero and age-appropriate normal cognitive functioning. The latter was based on a neuropsychological assessment battery that examined multiple domains, including episodic memory, attention, executive function, visuospatial processing, and language. Participants were classified as cognitively unimpaired by a team of neurologists and neuropsychologists, based on test scores falling within 1.5 standard deviations of demographically adjusted means; for details, see Trelle et al. (2020).

### 2.2. Image acquisition

MRI parameters for image acquisition are summarized in Table 2. Stanford participants were scanned with a 3D T1-weighted inversion-prepared fast spoiled gradient echo protocol at 3T and a WMnMPRAGE protocol at 7T, using 32-channel head coils in both cases. Bordeaux participants were imaged with 3D T1-weighted inversion-prepared fast spoiled gradient echo and WMnMPRAGE sequence protocols, both acquired at 3T using a 32-channel head coil.

T1-weighted images were acquired from Stanford older participants using the following scan parameters: 3T GE MR750 scanner, 3D BRAVO base sequence, sagittal acquisition, echo time (TE) 2.8 ms, repetition time (TR) 7.3 ms, inversion time (TI) 450 ms, flip angle

(FA) 12°, receive bandwidth (RBW) +/−41.67 kHz, spatial resolution 0.9 mm isotropic, 186 slices per volume, ARC parallel imaging acceleration: 1.75, scan time 4.8 min.

T1-weighted images were acquired from Stanford younger participants using the following scan parameters: 3T GE MR750 scanner, 3D MPRAGE base sequence, coronal acquisition, TE 3.9 ms, TR 8.5 ms, TI 1200 ms, sequence time (time between inversion pulses: TS) 3700 ms, FA 6°, RBW +/−19.2 kHz, spatial resolution 0.8 mm isotropic, 250 slices per volume, ARC parallel imaging acceleration: 3, scan time 4 min.

T1-weighted images were acquired from the Bordeaux cohort using one of two scan protocols: 1) for 22 participants of this cohort: 3T GE MR750w scanner, 3D BRAVO base sequence, sagittal acquisition, TE 3.2 ms, TR 8.5 ms, TI 400 ms, FA 11°, RBW +/−31.25 kHz, spatial resolution 1 mm isotropic, 180 slices per volume, scan time 10 min; or 2) for 16 participants of this cohort: 3T Canon Galan scanner, 3D MPRAGE base sequence, sagittal acquisition, TE 3.0 ms, TR 7.0 ms, TI 950 ms, FA 9°, RBW +/− 51.3 kHz, spatial resolution 0.6 mm isotropic, 234 slices per volume, SPEEDER parallel imaging acceleration: 1.5; scan time 4.5 min.

WMnMPRAGE images were acquired from all Stanford participants using the following parameters: 7T GE MR950 scanner, 3D MPRAGE base sequence, coronal acquisition, TE 4.6 ms, TR 10.1 ms, TI 680 ms, TS 5500 ms, views per segment 240, FA: 4°, RBW +/−11.9 kHz, spatial resolution 1 mm isotropic, 220 slices per volume, k-space ordering; 2D radial fanbeam, scan time 11.1 min.

WMnMPRAGE images were acquired from the Bordeaux cohort using one of two scan protocols: (1) for 22 participants of this cohort: 3T GE MR750w scanner, MPRAGE base sequence, coronal acquisition, TE 4.7 ms, TR 11.1 ms, TI 500 ms, TS 4500 ms, views per segment 240, FA: 7°, RBW +/− 11.9 kHz, spatial resolution 1 mm isotropic, 220 slices per volume k-space ordering; 2D radial fanbeam, ARC parallel imaging acceleration: 1.25×1.25, scan time 7.2 min; or (2) for 16 participants of this cohort: 3T Canon Galan scanner, 3D MPRAGE base sequence, axial acquisition, TE 3.6 ms, TR 7.8 ms, TI 470 ms, TS 4500 ms, FA 7°, RBW +/− 53.4 kHz, spatial resolution 0.8 mm isotropic, 200 slices per volume, SPEEDER parallel imaging acceleration: 1.3 × 1.6; scan time 11.3 min. See Saranathan et al. (2015) for further details.

T1-weighted and WMnMPRAGE image volumes were visually inspected to ensure that scans were of sufficient quality for analysis and were not corrupted by motion artifact.

### 2.3. Segmentations

Whole-brain WMnMPRAGE volumes were processed with the THOMAS thalamic segmentation tool with no preprocessing. The THOMAS algorithm applied to WMnMPRAGE images has been validated against manual segmentation (Su et al., 2019). Using version v0 of this tool (https://github.com/sujason/thomas), we segmented and extracted the volumes of 12 lateralized structures in each hemisphere of the brain: whole thalamus, ten thalamic nuclei (anteroventral [AV], centromedian [CM], lateral geniculate nucleus [LGN], mediodorsal [MD], medial geniculate nucleus [MGN], pulvinar [Pul],

ventral anterior [VA], ventral lateral anterior [VLA], ventral lateral posterior [VLP], and ventral posterolateral [VPL]), and one adjacent epithalamic structure, the habenula (Hb) (Fig. 1A). Note that THOMAS segments the whole thalamus separately from the thalamic nuclei; this whole thalamus encompasses all these preceding structures, as well as the mammillothalamic tract and some additional unlabeled thalamic areas (i.e., between segmented thalamic nuclei). See Tourdias et al. (2014), Saranathan et al. (2015), and Su et al. (2019) for additional details.

Whole-brain T1-weighted gradient echo volumes were processed with the FreeSurfer 7.1.1 pipeline with no preprocessing. Using the FreeSurfer tool SAMSEG (https://surfer.nmr.mgh.harvard.edu/fswiki/Samseg), we segmented and extracted the volumes of 11 structures on each side of the brain: nucleus accumbens, amygdala, caudate, cerebellar cortex, cerebellar white matter, cerebral cortex, cerebral white matter, hippocampus, lateral ventricle, pallidum, and putamen (Fig. 1B). SAMSEG produces volumes via both probabilistic and discrete voxel segmentation summations; we used the volumes calculated via the probabilistic method. The SAMSEG algorithm has been validated using T1-weighted images from different scanners and acquired with different scan parameters, using expert manual segmentation of these images as ground truth. SAMSEG was shown to have the highest average Dice score of the five segmentation methods studied (SAMSEG, FreeSurfer, PICSL MALF, BrainFuse, and majority voting) (Puonti et al., 2016). Note that SAMSEG produces a whole thalamus segmentation, but we used the THOMAS segmentation of the whole thalamus because it includes the LGN and MGN, two major thalamic nuclei, whereas the SAMSEG whole thalamus does not. In addition, the thalamic contrast is higher in WMnMPRAGE images than in conventional T1-weighted images; thus we expect the THOMAS segmentation of thalamic boundaries to be more accurate.

Intracranial volume (ICV) estimates were obtained from 3T whole-brain T1-weighted gradient echo volumes using SPM12's Segment and Tissue Volume Utility modules (https://www.fil.ion.ucl.ac.uk/spm/software/spm12) (Malone et al., 2015) (Fig. 1C). The accuracy of all segmentations was checked visually for each subject.

## 2.4. Statistical analyses

For each structure in the left and right hemispheres, we employed an exponential regression model to quantify the association between brain structural volume and age, adjusting for education, cohort, sex, and ICV, yielding the rate of age-related atrophy. In particular, we estimated the volume of each structure as a function of age, years of education, cohort, sex, and ICV using the following model:

$$E(Y \mid age,\ education,\ cohort,\ sex,\ ICV) = \exp(\beta_0 + \beta_1 age\ + \beta_2 education + \beta_3 cohort + \beta_4 sex + \gamma_1 \log ICV) = exp(\beta_0 + \beta_1 age\ + \beta_2 education + \beta_3 cohort\ + \beta_4 sex) \times \mathrm{ICV}^{\gamma 1},$$

which is equivalent to

$$E\left(\frac{Y}{ICV^{\gamma 1}} \mid age,\ education,\ cohort,\ sex\right)$$
$$= exp(\beta_0 + \beta_1 age + \beta_2 education + \beta_3 cohort + \beta_4 sex),$$

where $Y$ is the volume; education is in years; cohort = 0 for Stanford and 1 for Bordeaux, sex = 0 for female and 1 for male; and ICV is the total intracranial volume. Note: our principal analysis did not include education and cohort as covariates, but we did examine the influence of including these variables on our primary conclusions, described in more detail in Results and Discussion sections. An advantage of this exponential regression model is that the structure's relative (percent) volumetric change per year (defined as atrophy rate) is constant over the lifespan and represented by $\exp(\beta_1) - 1$. A Wald test was performed to test against the null hypothesis that there is no association between volumetric change and age (i.e., $H_0 : \beta_1 = 0$). In the Wald test, the standard error of the estimated coefficient was assessed by nonparametric bootstrap. We compared the atrophy rates of two structures by estimating the difference in the $\beta_1$ coefficients from the regression models of the two structures. The standard error of the estimated difference was assessed by nonparametric bootstrap, accounting for correlations between the volumes of structures from the same individual. Significant differences between the atrophy rates of structures were assessed with paired t-tests, adjusted for multiple comparisons. Hemisphere- and sex-specific differences in atrophy rates were similarly assessed by comparing the corresponding regression coefficients of age.

For the analysis assessing the functional specificity of thalamic nuclei atrophy, we grouped thalamic nuclei into six broad functional groups, based on their known anatomical connectivity (Steriade et al., 1997); that is, based on the known functions of the brain regions connected to each nucleus. These broad functional groups are cognitive (left+right AV and MD), visual (left+right LGN and pulvinar), auditory and vestibular (left+right MGN), motor (left+right VA, VLA, VLP, and CM), and somatosensory (left+right VPL). For the proximity-to-CSF analysis, we grouped thalamic nuclei into two groups based on their proximity to the nearest ventricular surface: an "adjacent" group (left+right AV, MD, MGN, LGN, and pulvinar) and a "remote" group (left+right CM, VA, VLA, VLP, and VPL). For each of these group analyses, we summed the volumes of all nuclei within a group and across both hemispheres, to create a single "composite" volume, and fit this composite volume with our regression model to obtain its atrophy rate. We then performed the Wald test against the null hypothesis that the atrophy rate was zero, and pairwise comparisons between groups to test for differences in their atrophy rates.

To adjust for multiple comparisons, the simultaneous confidence region for parameters of interest (e.g., regression coefficient of age corresponding to a group of structural volumes of interest) was constructed, where the covariance between relevant estimates was estimated by nonparametric bootstrap, and the corresponding p-values controlling the family-wise error rate via the supremum Wald test statistic were reported. The statistical analyses were conducted using R 4.1.1 (The R Foundation for Statistical Computing).

### 2.5. Data/code availability statement

Data and code are available upon request.

## 3. Results

### 3.1. Different thalamic nuclei show widely different age-related atrophy rates across the cognitively unimpaired adult lifespan

We found significant age-related atrophy of most of the thalamic nuclei (Fig. 2). Absolute thalamic nuclear volumes varied approximately linearly with age and with different atrophy rates for different nuclei. The following lists the THOMAS structures in descending order of annualized atrophy rate (Table 3). Left hemisphere: AV (1.18%), LGN (0.72%), MGN (0.67%), pulvinar (0.65%), CM (0.62%) VA (0.51%), MD (0.43%), VPL (0.36%), and VLP (0.30%). Right hemisphere: AV (1.08%), LGN (0.77%), CM (0.62%), MGN (0.61%), pulvinar (0.58%), VA (0.50%), MD (0.40%), VLP (0.34%), and VPL (0.28%). Atrophy rates of left and right VLA and habenula were not significantly different from zero. AV was notable in having a significantly greater atrophy rate than all other ipsilateral thalamic nuclei, except for the LGN in the right hemisphere (Supp. Fig. 1). These atrophy rates were not significantly changed after adjusting for years of education or cohort (Supp. Fig. 2). We also qualitatively observed that the older cohort had higher atrophy rates compared to those of the younger cohort (Fig. 2). We therefore assessed whether the atrophy rates for younger (Bordeaux and Stanford) or older cohorts differed from those of the whole group. We found that the younger cohorts together showed low, mostly non-significant atrophy rates, while the older cohort showed mostly significant atrophy rates that were similar to those of the whole group (Supp. Fig. 4 and Supp. Table 1).

### 3.2. The atrophy of thalamic nuclei segregates by function

We next examined whether the atrophy rates of thalamic nuclei were specific to function. This was hypothesized based on literature demonstrating that age-related atrophy occurs heterogeneously across functionally distinct cortical areas, with the greatest atrophy seen in frontal and temporal cortices and the least atrophy seen in sensorimotor and occipital cortices (Fjell and Walhovd, 2010; Fjell et al., 2009a; Raz et al., 1997). Thalamic nuclei were grouped into broad functional groups: cognitive (AV and MD), visual (LGN and pulvinar), auditory and vestibular (MGN), motor (VA, VLA, VLP, and CM), and somatosensory (VPL). We found a significant segregation of atrophy rates by function. The cognitive, visual, and auditory/vestibular groups showed the strongest atrophy rates, which ranged from 0.53% to 0.64% (Table 4). These were significantly different (adjusted $p<0.006$; Table 5) from the atrophy rates of the motor and somatosensory groups, which were 0.37% and 0.32%, respectively.

### 3.3. Thalamic nuclei that are adjacent to the ventricles show greater age-related atrophy

Prior work has found evidence in multiple sclerosis that thalamic nuclei adjacent to the ventricles show greater atrophy than nuclei that are located farther away from the ventricles (Lassmann, 2018; Planche et al., 2020). Here, we examined whether there was evidence that a similar effect occurs in cognitively unimpaired aging. To test this, thalamic nuclei

were grouped into two groups – those that were adjacent to the ventricles (AV, MD, LGN, pulvinar, and MGN) and those that were non-adjacent (i.e., remote) to the ventricles (CM, VA, VLA, VLP, and VPL). We found a significant difference of atrophy rates based on ventricular proximity: the adjacent group showed a higher atrophy rate (0.59% per year), which was significantly different (adjusted $p<0.001$) from that of the remote group (0.36% per year).

### 3.4. The thalamus and its nuclei have a high rate of atrophy in comparison to other brain structures across the cognitively unimpaired adult lifespan

For the extra-thalamic structures, we found that the absolute volumes of certain gray matter structures decreased approximately linearly with age, those of white matter structures did not significantly change with age, and those of the lateral ventricles increased nonlinearly with age (Fig. 3). Fig. 4 shows the percent change in volume per year for each structure; Table 3 shows these atrophy rates and their confidence bounds and p-values, adjusted for multiple comparisons. These atrophy rates were not significantly changed after adjusting for years of education or cohort (Supp. Fig. 2).

Significant differences between atrophy rates were assessed with paired t-tests, adjusted for multiple comparisons (Supp. Fig. 3). Notably, the left and right whole thalamic atrophy rates were higher than those of all extra-thalamic structures with the exception of the nucleus accumbens. Specifically, the atrophy rate of the left thalamus (0.45%) was significantly greater than that of all other significantly atrophying structures in the left hemisphere (Table 3), those being cerebellar cortex (0.24%), putamen (0.19%), and cerebral cortex (0.15%). The exception to this was the left nucleus accumbens (0.44%), which had an atrophy rate similar to (but not significantly different from) that of the left thalamus. The following left hemispheric structures had no statistically significant atrophy with age: cerebral white matter, cerebellar white matter, amygdala, hippocampus, caudate, and pallidum. We note that we do observe significant atrophy of these structures in the older cohort alone (Supp. Table 1). Similarly, the atrophy rate of the right thalamus (0.45%) was significantly greater than all other significantly atrophying right hemispheric structures, those being putamen (0.29%), cerebellar cortex (0.25%), caudate (0.21%), and cerebral cortex (0.15%). The exception to this was the right nucleus accumbens, whose atrophy rate (0.54%) was similar to that of the right thalamus. The following right hemispheric structures had no statistically significant atrophy with age: cerebral white matter, cerebellar white matter, amygdala, hippocampus, and pallidum; again, we note that the atrophy rates of these structures are significantly greater than zero when analyzing the older cohort alone (Supp. Table 1). Roughly half of the thalamic nuclei had higher rates of atrophy than all of the extra-thalamic structures examined in both the left and right hemispheres (Fig. 4).

We also found that the left and right lateral ventricles significantly *increased* in volume with age (left: 1.74% volume increase per year; right: 1.61%). The volumetric expansion of the lateral ventricle was nonlinear with age, increasing strongly for ages greater than 60 years.

### 3.5. Virtually no hemispheric or sex differences in the age-dependent changes of thalamic and extra-thalamic structures

Based on pairwise t-tests between the left and right volumes for each nucleus, adjusted for multiple comparisons, we did not observe any significant hemisphere-specific differences in atrophy rates for any thalamic or extra-thalamic structures.

Sex was entered as an independent variable in the exponential regression models described above for both intra- and extra-thalamic structures. Only one structure showed a sex-specific difference in atrophy rate. For the left CM nucleus of the thalamus, male participants showed a significantly greater atrophy rate than female participants (male, 0.86%; female, 0.41%; $p = 0.034$, adjusted for multiple comparisons).

## 4. Discussion

Prior literature examining the volumetric changes of brain structures during aging has consistently reported that the thalamus, along with other brain structures, significantly atrophies with age (Cherubini et al., 2009; Coupé et al., 2017; Narvacan et al., 2017; Raji et al., 2009; Walhovd et al., 2005, 2011; Zheng et al., 2019). Our principal finding is that thalamic nuclei have high and heterogeneous atrophy rates during cognitively unimpaired aging. Our results further suggest that a number of thalamic nuclei atrophy at greater rates than most of the extra-thalamic structures examined here. The high atrophy rates of thalamic nuclei may be the result of several underlying causes. One involves the “metabolism hypothesis”, proposed in the context of cortical hubs, which are brain regions with high degrees of connectivity and integration of information. Neuroimaging work has shown that these cortical hubs overlap with disease loci in Alzheimer’s disease – sites of amyloid beta deposition and hypometabolism (Buckner et al., 2009; Drzezga et al., 2011). The metabolism hypothesis proposes that cortical hubs are susceptible to disease due to their high levels of neuronal activity, which demand high levels of metabolism and create an excess of harmful free radical byproducts as well as pathological changes in gene and protein expression (Buckner et al., 2008, 2005). Similarly, the highly connected and integrative role of thalamic nuclei may make them susceptible to metabolic and molecular changes that disrupt normal neuronal processes and ultimately lead to structural changes.

Another hypothesis is that nuclei adjacent to ventricles may be more susceptible or accessible to CSF-mediated factors or immune cells that cause tissue damage and subsequent structural atrophy. Such CSF-mediated damage has been reported in multiple sclerosis (De Meo et al., 2022; Lassmann, 2018; Planche et al., 2020; Blyau et al., 2022) and recently in traumatic brain injury (Sandry and Dobryakova, 2021). We speculate that the same may occur in healthy aging. Indeed, our analysis shows that thalamic nuclei that are adjacent to ventricular surfaces (AV, MD, MGN, LGN, and pulvinar) atrophy at significantly higher rates than those that are more remote from CSF (CM, VA, VLA, VLP, and VPL), supporting the CSF-mediated damage hypothesis and providing the first evidence of this proximity-to-CSF hypothesis in healthy aging.

We note an alternative hypothesis to the proximity-to-CSF hypothesis that could also explain our observations. Our analysis of the functional specificity of thalamic atrophy rates showed

that cognitive, visual, and auditory/vestibular nuclei exhibited higher atrophy rates than the sensorimotor nuclei. However, these functional groupings are also consistent with the proximity-to-CSF groupings, with the cognitive, visual, and auditory/vestibular nuclei in the adjacent group and the sensorimotor nuclei in the remote group. With the present data and analyses, we are unable to lend support for one hypothesis over the other; indeed, the biology underlying volumetric atrophy of thalamic nuclei is undoubtedly complex and may allow for both hypotheses.

Despite the observed significant decline in thalamic volumes with age, all participants in our study had normal cognitive function. What might explain this finding? One possibility is that the brain can compensate for structural/volumetric changes via alternative circuitry, at least up to a point, such that cognition is largely preserved (Park and Reuter-Lorenz, 2009). Postmortem histological and patient neuroimaging studies indicate that thalamic volumes, as well as those of other brain structures, are smaller for patients with a variety of neurological conditions than for cognitively unimpaired age-matched control participants (Azevedo et al., 2018; Bishop et al., 2017; Callen et al., 2001; Cash et al., 2018; Fischl et al., 2002; Jernigan et al., 1991; Lee et al., 2020; Li et al., 2013; Schönecker et al., 2018). Thus, while there is significant observable atrophy in the cognitively unimpaired aged brain, an even greater amount of atrophy occurs in the diseased brain and may be necessary before observable clinical signs occur (Fjell and Walhovd, 2010). Alternatively, the atrophy observed in the cognitively unimpaired aged versus diseased brains may reflect different underlying biological processes. For example, neurodegenerative disease-related atrophy typically involves neurotoxic proteins and neuronal death. However, studies of cognitively unimpaired aging suggest that age-related atrophy generally does not involve neuronal death, but rather a shrinkage in neuronal size and reductions of the neuropil (see Fjell and Walhovd 2010 for review).

With the recent development of advanced thalamic segmentation methods (Iglesias et al., 2018; Su et al., 2019), studies have begun to show that specific thalamic nuclei are altered in disease (Aleman-Gomez et al., 2020; Bocchetta et al., 2020; Chipika et al., 2020; Huang et al., 2020; Jonak et al., 2020; Lee et al., 2020; Low et al., 2019; Planche et al., 2020; Shin et al., 2019). Several studies have also found evidence of volumetric differences in thalamic nuclei between asymptomatic genetic carriers and non-carriers in frontotemporal dementia (Bocchetta et al., 2021) and their association with PET-based levels of amyloid and tau in Alzheimer's disease (Pardilla-Delgado et al., 2021), highlighting the possibility that the volumes of thalamic nuclei may represent preclinical markers for disease. In our study, AV was the brain structure with the highest atrophy rate. We note that while the THOMAS method segments AV, this segmentation likely also includes some or all of the small, adjacent anterodorsal (AD) nucleus. The strong age-related atrophy of the AV nucleus observed in our study is consistent with prior work showing that anterior thalamic structures are implicated in Alzheimer's disease (Aggleton et al., 2016; Braak and Braak, 1991a). Postmortem histology shows that the AD nucleus is abnormal relatively early in Alzheimer's disease, with dense neurofibrillary tangles observed in stages II-III of the disease (Braak et al., 1996). AV is spared early in the disease, but sustains amyloid deposition in later stages of the disease (Braak and Braak, 1991a, b). Thus, our observation of AV's strong atrophy in this cognitively unimpaired sample may be an early indicator of processes contributing

to the development of Alzheimer's disease. Future studies are needed to longitudinally correlate the atrophy of AV and other thalamic nuclei with functional and disease markers, such as neuropsychological test scores, fMRI or PET activity, or cerebrospinal fluid levels of disease-related proteins, such as amyloid beta and tau.

We observed no hemisphere-specific differences and almost no sex-specific differences in age-related thalamic atrophy. There has been disagreement in the literature concerning the existence of hemisphere-specific (Hughes et al., 2012; Pieperhoff et al., 2008; Serbruyns et al., 2015; Squarzoni et al., 2018; Walhovd et al., 2011; Xu et al., 2000) or sex-specific (Coupé et al., 2017; Fjell et al., 2009b; Goodro et al., 2012; Király et al., 2016; Li et al., 2014; Murphy et al., 1996; Sullivan et al., 2004; Wang et al., 2019; Xu et al., 2000) differences in whole thalamic atrophy rates. Discrepancies may arise due to methodological differences between the studies, such as the sample size, ethnic background of the participants, and differing accuracies of the segmentation methods. In the present study, using a comparatively large sample size and the most accurate existing method for automatically segmenting thalamic nuclei, our data show virtually no hemisphere- or sex-specific differences in age-dependent atrophy rates for either the whole thalamus or individual thalamic nuclei. Future studies with larger sample sizes and state-of-the-art thalamic segmentation methods are needed to systematically tease apart thalamic atrophy in the context of different demographic factors, genetic backgrounds, and cognitive capabilities.

Although the focus of our study was on thalamic nuclei, we note several differences in the atrophy of some extra-thalamic structures compared to prior literature. We observed low or no significant atrophy of cerebral and cerebellar white matter and the hippocampus over the adult lifespan. Coupé et al. (2017) examined volumetric changes in a survey of brain structures (including the whole thalamus, but not thalamic nuclei) during development and over the adult lifespan and found robust cerebral and cerebellar white matter atrophy and moderate hippocampal atrophy over the older age range (>60 years), while for these brain regions the average atrophy rate over the middle age range (20–60) was near zero. Our data showed similar trends, with near-zero atrophy rates when the entire age range was analyzed, but increased atrophy rates (cerebral and cerebellar white matter: 0.14% to 0.31% per year; hippocampus: 0.48% to 0.57% per year; Supp. Fig. 4B; Supp. Table 1) when only the older age range was analyzed. Similar (though not as extreme) observations of increased atrophy rates in the older cohort compared to the full cohort were seen for other brain structures (Supp. Fig. 4B). Notwithstanding these nonlinear effects, the thalamus and its nuclei remain among the highest atrophying structures with age, even in the older cohort. Future studies will need to examine this issue using a larger number of participants analyzed with both the SAMSEG and volBrain pipelines.

### 4.1. Caveats and limitations

In the present study, we combined an older cohort with two younger cohorts to create a large sample spanning seven decades of adult age. As a result, there were several group-specific differences in scan acquisition parameters, such as scan protocol, field strength, and institution. For example, the WMnMPRAGE imaging for the Stanford younger and

older adults was acquired at 7T, while for the Bordeaux younger adults the WMnMPRAGE imaging was obtained at 3T. We first note that our analysis of brain volumes made exclusive use of fractional (or relative) volumes; this means that we analyzed only brain volumes normalized by ICV. We also adjusted for ICV in all regression analyses. Brain volumes and ICVs were obtained using the same segmentation tools for all participants. Therefore, if there is a multiplicative scaling bias as a result of a site-specific field strength, scanner, or software effect, then this scaling bias would be canceled in the formation of the fractional volumes. To further rule out a significant influence of field strength or institution, we tested for thalamic volume differences between Stanford (7T) and Bordeaux (3T) participants within the same age group and found no significant differences. We also found a similar pattern of atrophy after adjusting for cohort (Supp. Fig. 2B) or after analyzing solely the Stanford cohort (single site, same field strength) (Supp. Fig. 2C).

In addition, while the education level of our study population was uniformly high (mean 17.8 years, standard deviation 2.6 years), the older cohort had a somewhat lower group education level (mean 16.7 years) compared to the younger cohorts (mean 20.8 years). It is known that education level correlates with brain health and performance of certain cognitive abilities (Capitani et al., 2009; Mortiner, 1988). Indeed, Trelle et al. (2020) reported poorer episodic memory retrieval with lower education level in the present older cohort. Thus, we may have observed lower age-related atrophy rates if our average education levels had been more similar between the younger and older age cohorts. However, we found a similar pattern of atrophy across brain structures when we adjusted for years of education in our regression analysis (Supp. Fig. 2A and B). Thus, the confound of varying education level did not significantly impact the observed atrophy rates across the adult lifespan. Nonetheless, future work should include longitudinal studies following the same participants as they age to obtain more sensitive and controlled data on the atrophy of the thalamus and its nuclei with aging.

As an alternative to THOMAS, Iglesias et al. (2018) have created a thalamic nuclear segmentation method that is available in the FreeSurfer package. While the FreeSurfer thalamic segmentation method has a number of advantages, such as operating on conventional T1 images and offering segmentations of 25 nuclei, we used WMnMPRAGE and THOMAS in the present study, motivated by prior work (Majdi et al., 2020; Su et al., 2019) showing that the combination of WMnMPRAGE imaging and THOMAS segmentation results in higher accuracy in defining the boundaries of thalamic nuclei (as measured by Dice and VSI overlap metrics) compared to that obtained with the FreeSurfer method.

In the present study, we used two different methods to segment structural volumes –THOMAS for thalamic nuclei using WMnMPRAGE images and SAMSEG for extra-thalamic structures using conventional T1-weighted images. This approach was unavoidable, as no single method produces both sets of segmentations. Consequently, we note that there may be systematic software-specific effects that could affect comparisons between the atrophy rates of thalamic versus extra-thalamic structures. We note, however, that both THOMAS-derived and SAMSEG-derived whole thalamus volumes showed significant non-

zero atrophy with age (0.45% per year for THOMAS, 0.23% per year for SAMSEG), indicating comparable volumetry for these two segmentation methods.

Another caveat is that we compared brain structures of very differently sized volumes: the smallest structures we analyzed (habenula with an average volume of 25 $mm^3$) were almost 10,000 times smaller in volume than the largest structures (cerebral cortex with an average volume of nearly 250,000 $mm^3$). This huge dynamic range is the reason that we used an exponential model whose fundamental characteristic is a constant percent change in volume per unit time over the lifespan, allowing us to directly compare the relative atrophy rates of small and large structures; however, this did constrain our analysis to one particular nonlinear model. That said, our principal findings about the age-related atrophy rates of thalamic nuclei would not be affected by this issue, as the thalamic nuclei are relatively similar in volume. Future studies that more closely compare thalamic and extra-thalamic atrophy would likely benefit from examining subregions of large structures, such as cortical areas within the cerebral cortex.

Prior studies examining linear and nonlinear models of thalamic volume changes versus age have generally found linear relationships (Fjell et al., 2013; Goodro et al., 2012; Hasan et al., 2011; Sullivan et al., 2004). A few recent studies have reported nonlinear relationships (Coupé et al., 2017; Narvacan et al., 2017; Tullo et al., 2019; Wang et al., 2019). Using an exponential model with the capability of modeling linear and nonlinear atrophy, we also observed a consistently near-linear decrease throughout the adult lifespan. However, we note that our sample was not uniformly distributed over the age range – we had fewer participants in the 50–60 year age range, which is an age at which certain cognitive abilities such as verbal memory and visuospatial processing begin to decline (Salthouse, 2009; Schaie, 2005). Similarly, we note that while certain structures (e.g., whole thalamus, AV, and nucleus accumbens) clearly showed a near-linear reduction of volume throughout the age-span, this linearity is not so clear for other structures (e.g., cerebral and cerebellar cortices) as a result of a higher degree of scatter in our cross-sectional dataset, combined with the non-uniform sample distribution. These limitations could be addressed in future longitudinal studies with more participants, ideally distributed uniformly over the lifespan, to better detect any potential nonlinearities in the age-related atrophy of thalamic nuclear volumes.

Finally, the cross-sectional design adopted here is susceptible to variation in the volumes of these structures between individuals and does not provide a direct measure of within-individual age-related atrophy. Nonetheless, the present findings provide important initial evidence for heterogenous rates of volume loss among thalamic nuclei across the lifespan, a pattern that should be confirmed in future longitudinal studies.

## 5. Conclusions

Here, we showed that the thalamic nuclei have high and heterogeneous age-related atrophy in the cognitively unimpaired human brain. Thalamic nuclei involved in cognition (AV, MD), visual/visual association (LGN, pulvinar), and auditory/vestibular (MGN) function showed the highest atrophy rates. These five nuclei also happen to be adjacent to a ventricular surface, which may make them susceptible to CSF-mediated factors that affect brain

structure. The next tier of atrophy rates involved the nuclei related to motor (VA, VLA, VLP, and CM) and somatosensory (VPL) functions, and these five nuclei happen to be located at some distance from the nearest ventricular surface. We found no significant hemispheric, sex-specific, or education-specific differences in these rates of change for thalamic nuclei. These results provide a baseline measure of atrophy rates occurring in thalamic nuclei across the cognitively unimpaired adult lifespan. Given that our participants were all cognitively unimpaired, our results indicate the range of structural atrophy that can be tolerated by the resilient cognitively unimpaired aged brain while preserving cognitive functioning. These findings indicate that the thalamus and its nuclei are a component of age-related brain atrophy in the cognitively unimpaired human brain. A detailed understanding of such atrophy may provide insights into the transition from cognitively unimpaired brain aging to pathological neurodegeneration and other neurological and psychiatric disease.

## Supplementary Material

Refer to Web version on PubMed Central for supplementary material.

## Acknowledgements

We thank the following individuals for their contributions to data collection: Jeff Bernstein, Nicole Corso, Wanjia Guo, Madison Hunt, Manasi Jayakumar, Anna Khazenzon, Celia Litovsky, Hannah Lloyd, Ayesha Nadiadwala, Natalie Tanner, and Monica Thieu. We also thank Dr. Garrett Drayna for expert technical assistance and discussion. This work was supported by the National Institutes of Health (P30 AG066515, P41 EB01589125, R01 AG048076, R01 AG065255, R21 AG058111, R21 AG058859, UH3 NS095554, UL1 TR003142), Department of Defense (W81XWH-20-PRARP-CSRA), Alzheimer's Association (AARFD-21-852597), Stanford Precision Health and Integrated Diagnostic Center (PHIND), Stanford Wu Tsai Neurosciences Institute, Stanford Center for Clinical and Translational Education and Research (Spectrum), GE Healthcare, ARSEP Foundation, and Idex Bordeaux University (IMPACT program).

## Data/code availability statement

Data and code are available upon request.

## Data Availability

Data will be made available on request.

## Abbreviations:

| | |
|---|---|
| **THOMAS** | THalamus Optimized MultiAtlas Segmentation |

## References

Aggleton JP, Pralus A, Nelson AJ, Hornberger M, 2016. Thalamic pathology and memory loss in early Alzheimer's disease: moving the focus from the medial temporal lobe to Papez circuit. Brain 139, 1877–1890. [PubMed: 27190025]

Aleman-Gomez Y, Najdenovska E, Roine T, Fartaria MJ, Canales-Rodriguez EJ, Rovo Z, Hagmann P, Conus P, Do KQ, Klauser P, Steullet P, Baumann PS, Bach Cuadra M, 2020. Partial-volume modeling reveals reduced gray matter in specific thalamic nuclei early in the time course of psychosis and chronic schizophrenia. Hum. Brain Mapp. 41, 4041–4061. [PubMed: 33448519]

Azevedo CJ, Cen SY, Khadka S, Liu S, Kornak J, Shi Y, Zheng L, Hauser SL, Pelletier D, 2018. Thalamic atrophy in multiple sclerosis: a magnetic resonance imaging marker of neurodegeneration throughout disease. Ann. Neurol. 83, 223–234. [PubMed: 29328531]

Bishop CA, Newbould RD, Lee JS, Honeyfield L, Quest R, Colasanti A, Ali R, Mattoscio M, Cortese A, Nicholas R, Matthews PM, Muraro PA, Waldman AD, 2017. Analysis of ageing-associated grey matter volume in patients with multiple sclerosis shows excess atrophy in subcortical regions. Neuroimage Clin. 13, 9–15. [PubMed: 27896065]

Blyau S, Koubiyr I, Saranathan M, Coupé P, Deloire M, Charré-Morin J, Saubusse A, Zhang B, Rutt BK, Dousset V, Brochet B, Ruet A, Tourdias T, 2022. Differential vulnerability of thalamic nuclei in multiple sclerosis. Mult. Scler. J 1–6. doi:10.1177/13524585221114247.

Bocchetta M, Iglesias JE, Neason M, Cash DM, Warren JD, Rohrer JD, 2020. Thalamic nuclei in frontotemporal dementia: mediodorsal nucleus involvement is universal but pulvinar atrophy is unique to C9orf72. Hum. Brain Mapp. 41, 1006–1016. [PubMed: 31696638]

Bocchetta MTE, Peakman G, Cash DM, Convery RS, Russell LL, Thomas DL, Eugenio Iglesias J, van Swieten JC, Jiskoot LC, Seelaar H, Borroni B, Galimberti D, Sanchez-Valle R, Laforce R, Moreno F, Synofzik M, Graff C, Masellis M, Carmela Tartaglia M, Rowe JB, Vandenberghe R, Finger E, Tagliavini F, de Mendonça A, Santana I, Butler CR, Ducharme S, Gerhard A, Danek A, Levin J, Otto M, Sorbi S, Le Ber I, Pasquier F, Rohrer JD; Genetic Frontotemporal dementia Initiative (GENFI). 2021. Differential early subcortical involvement in genetic FTD within the GENFI cohort. Neuroimage 30, 102646. [PubMed: 33895632]

Braak H, Braak E, 1991a. Alzheimer's disease affects limbic nuclei of the thalamus. Acta Neuropathol. 81, 261–268. [PubMed: 1711755]

Braak H, Braak E, 1991b. Neuropathological stageing of Alzheimer-related changes. Acta Neuropathol. 82, 239–259. [PubMed: 1759558]

Braak H, Braak E, Yilmazer D, de Vos RA, Jansen EN, Bohl J, 1996. Pattern of brain destruction in Parkinson's and Alzheimer's diseases. J. Neural Transm. 103, 455–490. [PubMed: 9617789]

Buckner RL, Andrews-Hanna JR, Schacter DL, 2008. The brain's default network: anatomy, function, and relevance to disease. Ann. N. Y. Acad. Sci. 1124, 1–38. [PubMed: 18400922]

Buckner RL, Sepulcre J, Talukdar T, Krienen FM, Liu H, Hedden T, Andrews-Hanna JR, Sperling RA, Johnson KA, 2009. Cortical hubs revealed by intrinsic functional connectivity: mapping, assessment of stability, and relation to Alzheimer's disease. J. Neurosci. 29, 1860–1873. [PubMed: 19211893]

Buckner RL, Snyder AZ, Shannon BJ, LaRossa G, Sachs R, Fotenos AF, Sheline YI, Klunk WE, Mathis CA, Morris JC, Mintun MA, 2005. Molecular, structural, and functional characterization of Alzheimer's disease: evidence for a relationship between default activity, amyloid, and memory. J. Neurosci. 25, 7709–7717. [PubMed: 16120771]

Byne W, Buchsbaum MS, Mattiace LA, Hazlett EA, Kemether E, Elhakem SL, Purohit DP, Haroutunian V, Jones L, 2002. Postmortem assessment of thalamic nuclear volumes in subjects with schizophrenia. Am. J. Psychiatry 159, 59–65. [PubMed: 11772691]

Callen DJ, Black SE, Gao F, Caldwell CB, Szalai JP, 2001. Beyond the hippocampus: MRI volumetry confirms widespread limbic atrophy in AD. Neurology 57, 1669–1674. [PubMed: 11706109]

Capitani E, Barbarotto R, Laiacona M, 2009. Does education influence the age-related cognitive decline? A further inquiry. Dev. Neuropsychol. 12 (2), 231–240.

Carrera E, Bogousslavsky J, 2006. The thalamus and behavior: effects of anatomically distinct strokes. Neurology 66, 1817–1823. [PubMed: 16801643]

Cash DM, Bocchetta M, Thomas DL, Dick KM, van Swieten JC, Borroni B, Galimberti D, Masellis M, Tartaglia MC, Rowe JB, Graff C, Tagliavini F, Frisoni GB, Laforce R Jr., Finger E, de Mendonca A, Sorbi S, Rossor MN, Ourselin S, Rohrer JD, Genetic Ftd Initiative G, 2018. Patterns of gray matter atrophy in genetic frontotemporal dementia: results from the GENFI study. Neurobiol. Aging 62, 191–196. [PubMed: 29172163]

Cherubini A, Peran P, Caltagirone C, Sabatini U, Spalletta G, 2009. Aging of subcortical nuclei: microstructural, mineralization and atrophy modifications measured in vivo using MRI. Neuroimage 48, 29–36. [PubMed: 19540925]

Chipika RH, Siah WF, Shing SLH, Finegan E, McKenna MC, Christidi F, Chang KM, Karavasilis E, Vajda A, Hengeveld JC, Doherty MA, Donaghy C, Hutchinson S, McLaughlin RL, Hardiman O, Bede P, 2020. MRI data confirm the selective involvement of thalamic and amygdalar nuclei in amyotrophic lateral sclerosis and primary lateral sclerosis. Data Brief 32, 106246. [PubMed: 32944601]

Coupé P, Catheline G, Lanuza E, Manjon JV, 2017. Towards a unified analysis of brain maturation and aging across the entire lifespan: a MRI analysis. Hum. Brain Mapp. 38, 5501–5518. [PubMed: 28737295]

De Meo E, Portaccio E, Prestipino E, Nacmias B, Bagnoli S, Razzolini L, Pasto L, Niccolai C, Goretti B, Bellinvia A, Fonderico M, Giorgio A, Stromillo ML, Filippi M, Sorbi S, De Stefano N, Amato MP, 2022. Effect of BDNF Val66Met polymorphism on hippocampal subfields in multiple sclerosis patients. Mol. Psychiatry 27, 1010–1019. [PubMed: 34650209]

Drzezga A, Becker JA, Van Dijk KR, Sreenivasan A, Talukdar T, Sullivan C, Schultz AP, Sepulcre J, Putcha D, Greve D, Johnson KA, Sperling RA, 2011. Neuronal dysfunction and disconnection of cortical hubs in non-demented subjects with elevated amyloid burden. Brain 134, 1635–1646. [PubMed: 21490054]

Fama R, Sullivan EV, 2015. Thalamic structures and associated cognitive functions: relations with age and aging. Neurosci. Biobehav. Rev. 54, 29–37. [PubMed: 25862940]

Fischl B, Salat DH, Busa E, Albert M, Dieterich M, Haselgrove C, van der Kouwe A, Killiany R, Kennedy D, Klaveness S, Montillo A, Makris N, Rosen B, Dale AM, 2002. Whole brain segmentation: automated labeling of neuroanatomical structures in the human brain. Neuron 33, 341–355. [PubMed: 11832223]

Fjell AM, Walhovd KB, 2010. Structural brain changes in aging: courses, causes and cognitive consequences. Rev. Neurosci 21, 187–221. [PubMed: 20879692]

Fjell AM, Walhovd KB, Fennema-Notestine C, McEvoy LK, Hagler DJ, Holland D, Brewer JB, Dale AM, 2009a. One-year brain atrophy evident in healthy aging. J. Neurosci. 29, 15223–15231. [PubMed: 19955375]

Fjell AM, Westlye LT, Amlien I, Espeseth T, Reinvang I, Raz N, Agartz I, Salat DH, Greve DN, Fischl B, Dale AM, Walhovd KB, 2009b. Minute effects of sex on the aging brain: a multisample magnetic resonance imaging study of healthy aging and Alzheimer's disease. J. Neurosci. 29, 8774–8783. [PubMed: 19587284]

Fjell AM, Westlye LT, Grydeland H, Amlien I, Espeseth T, Reinvang I, Raz N, Holland D, Dale AM, Walhovd KB, 2013. Critical ages in the life course of the adult brain: nonlinear subcortical aging. Neurobiol. Aging 34, 2239–2247. [PubMed: 23643484]

Goodro M, Sameti M, Patenaude B, Fein G, 2012. Age effect on subcortical structures in healthy adults. Psychiatry Res. 203, 38–45. [PubMed: 22863654]

Hasan KM, Walimuni IS, Abid H, Frye RE, Ewing-Cobbs L, Wolinsky JS, Narayana PA, 2011. Multimodal quantitative magnetic resonance imaging of thalamic development and aging across the human lifespan: implications to neurodegeneration in multiple sclerosis. J. Neurosci. 31, 16826–16832. [PubMed: 22090508]

Huang AS, Rogers BP, Sheffield JM, Jalbrzikowski ME, Anticevic A, Blackford JU, Heckers S, Woodward ND, 2020. Thalamic Nuclei volumes in psychotic disorders and in youths with psychosis spectrum symptoms. Am. J. Psychiatry 177, 1159–1167. [PubMed: 32911995]

Hughes EJ, Bond J, Svrckova P, Makropoulos A, Ball G, Sharp DJ, Edwards AD, Hajnal JV, Counsell SJ, 2012. Regional changes in thalamic shape and volume with increasing age. Neuroimage 63, 1134–1142. [PubMed: 22846656]

Iglesias JE, Insausti R, Lerma-Usabiaga G, Bocchetta M, Leemput KV, Greve DN, van der Kouwe A, Fischl B, Caballero-Gaudes C, Paz-Alonso PM, 2018. A probabilistic atlas of the human thalamic nuclei combining ex vivo MRI and histology. Neuroimage 183, 314–326. doi:10.1016/j.neuroimage.2018.08.012. [PubMed: 30121337]

Jernigan TL, Salmon DP, Butters N, Hesselink JR, 1991. Cerebral structure on MRI, Part II: specific changes in Alzheimer's and Huntington's diseases. Biol. Psychiatry 29, 68–81. [PubMed: 1825793]

Jonak K, Krukow P, Jonak KE, Radzikowska E, Baj J, Niedzialek A, Pankowska A, Symms M, Stepniewski A, Podkowinski A, Osuchowska I, Grochowski C, 2020. Decreased volume of lateral and medial geniculate nuclei in patients with LHON disease–7 tesla MRI study. J. Clin. Med. 9, 2914–2928. [PubMed: 32927622]

Király A, Szabo N, Toth E, Csete G, Farago P, Kocsis K, Must A, Vecsei L, Kincses ZT, 2016. Male brain ages faster: the age and gender dependence of subcortical volumes. Brain Imaging Behav. 10, 901–910. [PubMed: 26572143]

Lassmann H, 2018. Pathogenic mechanisms associated with different clinical courses of multiple sclerosis. Front. Immunol. 9, 3116. [PubMed: 30687321]

Lee HJ, Seo SA, Park KM, 2020. Quantification of thalamic nuclei in patients diagnosed with temporal lobe epilepsy and hippocampal sclerosis. Neuroradiology 62, 185–195. [PubMed: 31673749]

Li W, van Tol MJ, Li M, Miao W, Jiao Y, Heinze HJ, Bogerts B, He H, Walter M, 2014. Regional specificity of sex effects on subcortical volumes across the lifespan in healthy aging. Hum. Brain Mapp. 35, 238–247. [PubMed: 22996803]

Li YD, He HJ, Dong HB, Feng XY, Xie GM, Zhang LJ, 2013. Discriminative analysis of early-stage Alzheimer's disease and normal aging with automatic segmentation technique in subcortical gray matter structures: a multicenter in vivo MRI volumetric and DTI study. Acta Radiol. 54, 1191–1200. [PubMed: 23878359]

Long X, Liao W, Jiang C, Liang D, Qiu B, Zhang L, 2012. Healthy aging: an automatic analysis of global and regional morphological alterations of human brain. Acad. Radiol. 19, 785–793. [PubMed: 22503890]

Low A, Mak E, Malpetti M, Chouliaras L, Nicastro N, Su L, Holland N, Rittman T, Rodriguez PV, Passamonti L, Bevan-Jones WR, Jones PS, Rowe JB, O'Brien JT, 2019. Asymmetrical atrophy of thalamic subnuclei in Alzheimer's disease and amyloid-positive mild cognitive impairment is associated with key clinical features. Alzheimer's Dement. 11, 690–699.

Majdi MS, Keerthivasan MB, Rutt BK, Zahr NM, Rodriguez JJ, Saranathan M, 2020. Automated thalamic nuclei segmentation using multi-planar cascaded convolutional neural networks. Magn. Reson. Imaging 73, 45–54. [PubMed: 32828985]

Malone IB, Leung KK, Clegg S, Barnes J, Whitwell JL, Ashburner J, Fox NC, Ridgway GR, 2015. Accurate automatic estimation of total intracranial volume: a nuisance variable with less nuisance. Neuroimage 104, 366–372. [PubMed: 25255942]

Morris JC, 1993. The Clinical Dementia Rating (CDR): current version and scoring rules. Neurology 43, 2412–2414.

Mortiner JA, 1988. Do psychosocial risk factors contribute to Alzheimer's disease? In: Hendersen AS, Hendersen JH (Eds.) Etiology of Dementia of Alzheimer's Type. John Wiley & Sons, Chichester, UK, pp. 39–52.

Murphy DG, DeCarli C, McIntosh AR, Daly E, Mentis MJ, Pietrini P, Szczepanik J, Schapiro MB, Grady CL, Horwitz B, Rapoport SI, 1996. Sex differences in human brain morphometry and metabolism: an in vivo quantitative magnetic resonance imaging and positron emission tomography study on the effect of aging. Arch. Gen. Psychiatry 53, 585–594. [PubMed: 8660125]

Murphy DG, DeCarli CD, Daly E, Gillette JA, McIntosh AR, Haxby JV, Teichberg D, Schapiro MB, Rapoport SI, Horwitz B, 1993. Volumetric magnetic resonance imaging in men with dementia of the Alzheimer type: correlations with disease severity. Biol. Psychiatry 34, 612–621. [PubMed: 8292690]

Narvacan K, Treit S, Camicioli R, Martin W, Beaulieu C, 2017. Evolution of deep gray matter volume across the human lifespan. Hum. Brain Mapp. 38, 3771–3790. [PubMed: 28548250]

Nyberg L, Salami A, Andersson M, Eriksson J, Kalpouzos G, Kauppi K, Lind J, Pudas S, Persson J, Nilsson LG, 2010. Longitudinal evidence for diminished frontal cortex function in aging. Proc. Natl. Acad. Sci. U. S. A. 107, 22682–22686. [PubMed: 21156826]

Pardilla-Delgado E, Torrico-Teave H, Sanchez JS, Ramirez-Gomez LA, Baena A, Bocanegra Y, Vila-Castelar C, Fox-Fuller JT, Guzman-Velez E, Martinez J, Alvarez S, Ochoa-Escudero M, Lopera F, Quiroz YT, 2021. Associations between subregional thalamic volume and brain pathology in autosomal dominant Alzheimer's disease. Brain Commun. 3, fcab101. [PubMed: 34095834]

Park DC, Reuter-Lorenz P, 2009. The adaptive brain: aging and neurocognitive scaffolding. Annu. Rev. Psychol. 60, 173–196. [PubMed: 19035823]

Pieperhoff P, Homke L, Schneider F, Habel U, Shah NJ, Zilles K, Amunts K, 2008. Deformation field morphometry reveals age-related structural differences between the brains of adults up to 51 years. J. Neurosci. 28, 828–842. [PubMed: 18216191]

Planche V, Su JH, Mournet S, Saranathan M, Dousset V, Han M, Rutt BK, Tourdias T, 2020. White-matter-nulled MPRAGE at 7T reveals thalamic lesions and atrophy of specific thalamic nuclei in multiple sclerosis. Mult. Scler. 26, 987–992. [PubMed: 30730233]

Popken GJ, Bunney WE Jr., Potkin SG, Jones EG, 2000. Subnucleus-specific loss of neurons in medial thalamus of schizophrenics. Proc. Natl. Acad. Sci. U. S. A. 97, 9276–9280. [PubMed: 10908653]

Puonti O, Iglesias JE, Van Leemput K, 2016. Fast and sequence-adaptive whole-brain segmentation using parametric Bayesian modeling. Neuroimage 143, 235–249. [PubMed: 27612647]

Raji CA, Lopez OL, Kuller LH, Carmichael OT, Becker JT, 2009. Age, Alzheimer disease, and brain structure. Neurology 73, 1899–1905. [PubMed: 19846828]

Raz N, Gunning FM, Head D, Dupuis JH, McQuain J, Briggs SD, Loken WJ, Thornton AE, Acker JD, 1997. Selective aging of the human cerebral cortex observed in vivo: differential vulnerability of the prefrontal gray matter. Cereb. Cortex 7, 268–282. [PubMed: 9143446]

Salthouse TA, 2009. Decomposing age correlations on neuropsychological and cognitive variables. J. Int. Neuropsychol. Soc. 15, 650–661. [PubMed: 19570312]

Sandry J, Dobryakova E, 2021. Global hippocampal and selective thalamic nuclei atrophy differentiate chronic TBI from Non-TBI. Cortex 145, 37–56. [PubMed: 34689031]

Saranathan M, Tourdias T, Bayram E, Ghanouni P, Rutt BK, 2015. Optimization of white-matter-nulled magnetization prepared rapid gradient echo (MP-RAGE) imaging. Magn. Reson. Med. 73, 1786–1794. [PubMed: 24889754]

Schaie KW, 2005. Developmental Influences on Adult Intelligence: The Seattle longitudinal study. Oxford University Press, Inc., New York, NY.

Schippling S, Ostwaldt AC, Suppa P, Spies L, Manogaran P, Gocke C, Huppertz HJ, Opfer R, 2017. Global and regional annual brain volume loss rates in physiological aging. J. Neurol. 264, 520–528. [PubMed: 28054131]

Schönecker S, Neuhofer C, Otto M, Ludolph A, Kassubek J, Landwehrmeyer B, Anderl-Straub S, Semler E, Diehl-Schmid J, Prix C, Vollmar C, Fortea J, Deutsches F-K, Huppertz HJ, Arzberger T, Edbauer D, Feddersen B, Dieterich M, Schroeter ML, Volk AE, Fliessbach K, Schneider A, Kornhuber J, Maler M, Prudlo J, Jahn H, Boeckh-Behrens T, Danek A, Klopstock T, Levin J, 2018. Atrophy in the thalamus but not cerebellum is specific for C9orf72 FTD and ALS patients - an atlas-based volumetric MRI study. Front. Aging Neurosci. 10, 45. [PubMed: 29599716]

Serbruyns L, Leunissen I, Huysmans T, Cuypers K, Meesen RL, van Ruitenbeek P, Sijbers J, Swinnen SP, 2015. Subcortical volumetric changes across the adult lifespan: subregional thalamic atrophy accounts for age-related sensorimotor performance declines. Cortex 65, 128–138. [PubMed: 25682047]

Shin KJ, Lee HJ, Park KM, 2019. Alterations of individual thalamic nuclei volumes in patients with migraine. J. Headache Pain 20, 112. [PubMed: 31818256]

Small SA, 2014. Isolating pathogenic mechanisms embedded within the hippocampal circuit through regional vulnerability. Neuron 84, 32–39. [PubMed: 25277453]

Squarzoni P, Duran FLS, Busatto GF, Alves T, 2018. Reduced gray matter volume of the thalamus and hippocampal region in elderly healthy adults with no impact of APOE varepsilon4: a longitudinal voxel-based morphometry study. J. Alzheimer's Dis. 62, 757–771. [PubMed: 29480170]

Steriade M, Jones EG, McCormick DA, 1997. Thalamus. Elsevier Science Ltd, Oxford, UK.

Su JH, Choi EY, Tourdias T, Saranathan M, Halpern CH, Henderson JM, Pauly KB, Ghanouni P, Rutt BK, 2020. Improved Vim targeting for focused ultrasound ablation treatment of essential tremor: a probabilistic and patient-specific approach. Hum. Brain Mapp. 41, 4769–4788. [PubMed: 32762005]

Su JH, Thomas FT, Kasoff WS, Tourdias T, Choi EY, Rutt BK, Saranathan M, 2019. Thalamus Optimized Multi Atlas Segmentation (THOMAS): fast, fully automated segmentation of thalamic nuclei from structural MRI. Neuroimage 194, 272–282. [PubMed: 30894331]

Su L, Wang L, Chen F, Shen H, Li B, Hu D, 2012. Sparse representation of brain aging: extracting covariance patterns from structural MRI. PLoS ONE 7, e36147. [PubMed: 22590522]

Sullivan EV, Rosenbloom M, Serventi KL, Pfefferbaum A, 2004. Effects of age and sex on volumes of the thalamus, pons, and cortex. Neurobiol. Aging 25, 185–192. [PubMed: 14749136]

Takahashi R, Ishii K, Kakigi T, Yokoyama K, 2011. Gender and age differences in normal adult human brain: voxel-based morphometric study. Hum. Brain Mapp. 32, 1050–1058. [PubMed: 20607753]

Tourdias T, Saranathan M, Levesque IR, Su J, Rutt BK, 2014. Visualization of intra-thalamic nuclei with optimized white-matter-nulled MPRAGE at 7T. Neuroimage 84, 534–545. [PubMed: 24018302]

Trelle AN, Carr VA, Guerin SA, Thieu MK, Jayakumar M, Guo W, Nadiadwala A, Corso NK, Hunt MP, Litovsky CP, Tanner NJ, Deutsch GK, Bernstein JD, Harrison MB, Khazenzon AM, Jiang J, Sha SJ, Fredericks CA, Rutt BK, Mormino EC, Kerchner GA, Wagner AD, 2020. Hippocampal and cortical mechanisms at retrieval explain variability in episodic remembering in older adults. eLife 9, e55335. doi:10.7554/eLife.55335. [PubMed: 32469308]

Trelle AN, Carr VA, Wilson EN, Swarovski MS, Hunt MP, Toueg TN, Tran TT, Channappa D, Corso NK, Thieu MK, Jayakumar M, Nadiadwala A, Guo W, Tanner NJ, Bernstein JD, Litovsky CP, Guerin SA, Khazenzon AM, Harrison MB, Rutt BK, Deutsch GK, Chin FT, Davidzon GA, Hall JN, Sha SJ, Fredericks CA, Andreasson KI, Kerchner GA, Wagner AD, Mormino EC, 2021. Association of CSF biomarkers with hippocampal-dependent memory in preclinical Alzheimer Disease. Neurology 96, e1470–e1481. [PubMed: 33408146]

Tullo S, Patel R, Devenyi GA, Salaciak A, Bedford SA, Farzin S, Wlodarski N, Tardif CL, Group P-AR, Breitner JCS, Chakravarty MM, 2019. MR-based age-related effects on the striatum, globus pallidus, and thalamus in healthy individuals across the adult lifespan. Hum. Brain Mapp. 40, 5269–5288. [PubMed: 31452289]

Van Der Werf YD, Tisserand DJ, Visser PJ, Hofman PA, Vuurman E, Uylings HB, Jolles J, 2001. Thalamic volume predicts performance on tests of cognitive speed and decreases in healthy aging. A magnetic resonance imaging-based volumetric analysis. Brain Res. Cogn. Brain Res. 11, 377–385. [PubMed: 11339987]

Walhovd KB, Fjell AM, Reinvang I, Lundervold A, Dale AM, Eilertsen DE, Quinn BT, Salat D, Makris N, Fischl B, 2005. Effects of age on volumes of cortex, white matter and subcortical structures. Neurobiol. Aging 26, 1261–1270. [PubMed: 16005549]

Walhovd KB, Westlye LT, Amlien I, Espeseth T, Reinvang I, Raz N, Agartz I, Salat DH, Greve DN, Fischl B, Dale AM, Fjell AM, 2011. Consistent neuroanatomical age-related volume differences across multiple samples. Neurobiol. Aging 32, 916–932. [PubMed: 19570593]

Wang Y, Xu Q, Luo J, Hu M, Zuo C, 2019. Effects of age and sex on subcortical volumes. Front. Aging Neurosci. 11, 259. [PubMed: 31616285]

Xu J, Kobayashi S, Yamaguchi S, Iijima K, Okada K, Yamashita K, 2000. Gender effects on age-related changes in brain structure. AJNR Am. J. Neuroradiol. 21, 112–118. [PubMed: 10669234]

Yoo HB, De Ridder D, Vanneste S, 2016. The importance of aging in gray matter changes within tinnitus patients shown in cortical thickness, surface area and volume. Brain Topogr. 29, 885–896. [PubMed: 27509900]

Young KA, Manaye KF, Liang C, Hicks PB, German DC, 2000. Reduced number of mediodorsal and anterior thalamic neurons in schizophrenia. Biol. Psychiatry 47, 944–953. [PubMed: 10838062]

Zahr NM, Sullivan EV, Pohl KM, Pfefferbaum A, Saranathan M, 2020. Sensitivity of ventrolateral posterior thalamic nucleus to back pain in alcoholism and CD4 nadir in HIV. Hum. Brain Mapp. 41, 1351–1361. [PubMed: 31785046]

Zheng F, Liu Y, Yuan Z, Gao X, He Y, Liu X, Cui D, Qi R, Chen T, Qiu J, 2019. Age-related changes in cortical and subcortical structures of healthy adult brains: a surface-based morphometry study. J. Magn. Reson. Imaging 49, 152–163. [PubMed: 29676856]

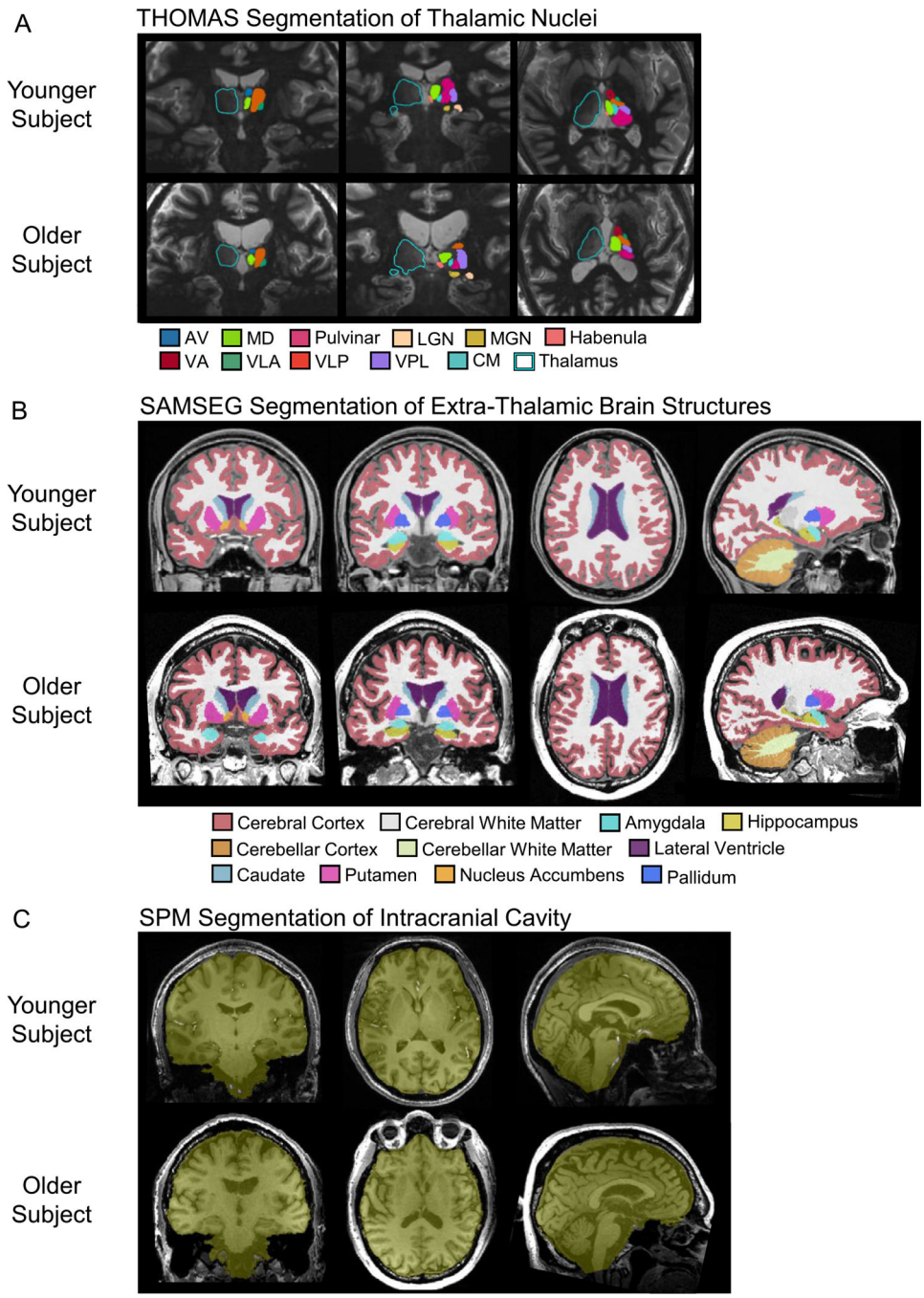


**Fig. 1.**

Segmentations in representative younger and older subjects. (A) Whole thalamus, thalamic nuclei, and habenula segmentations using THOMAS and white matter-nulled MPRAGE imaging. (B) Extra-thalamic segmentations using FreeSurfer's SAMSEG tool. (C) Intracranial cavity segmentation using SPM12's Segment and Tissue Volume Utility modules.

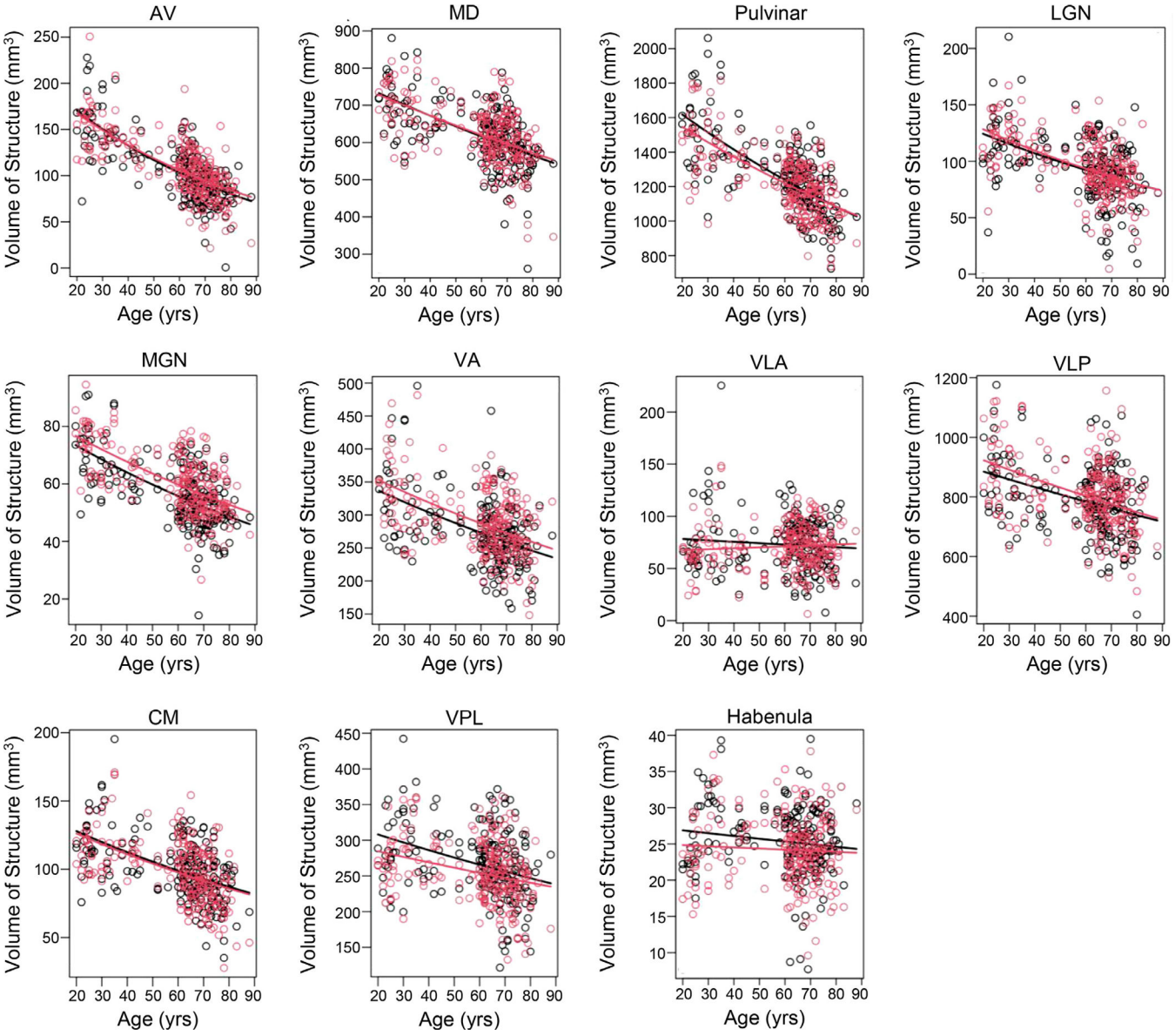


**Fig. 2.**

Absolute volumes of THOMAS-derived thalamic structures plotted versus age, showing heterogeneous atrophy between nuclei. Curves show best fits to the defined exponential regression model. Red=right hemisphere. Black=left hemisphere.

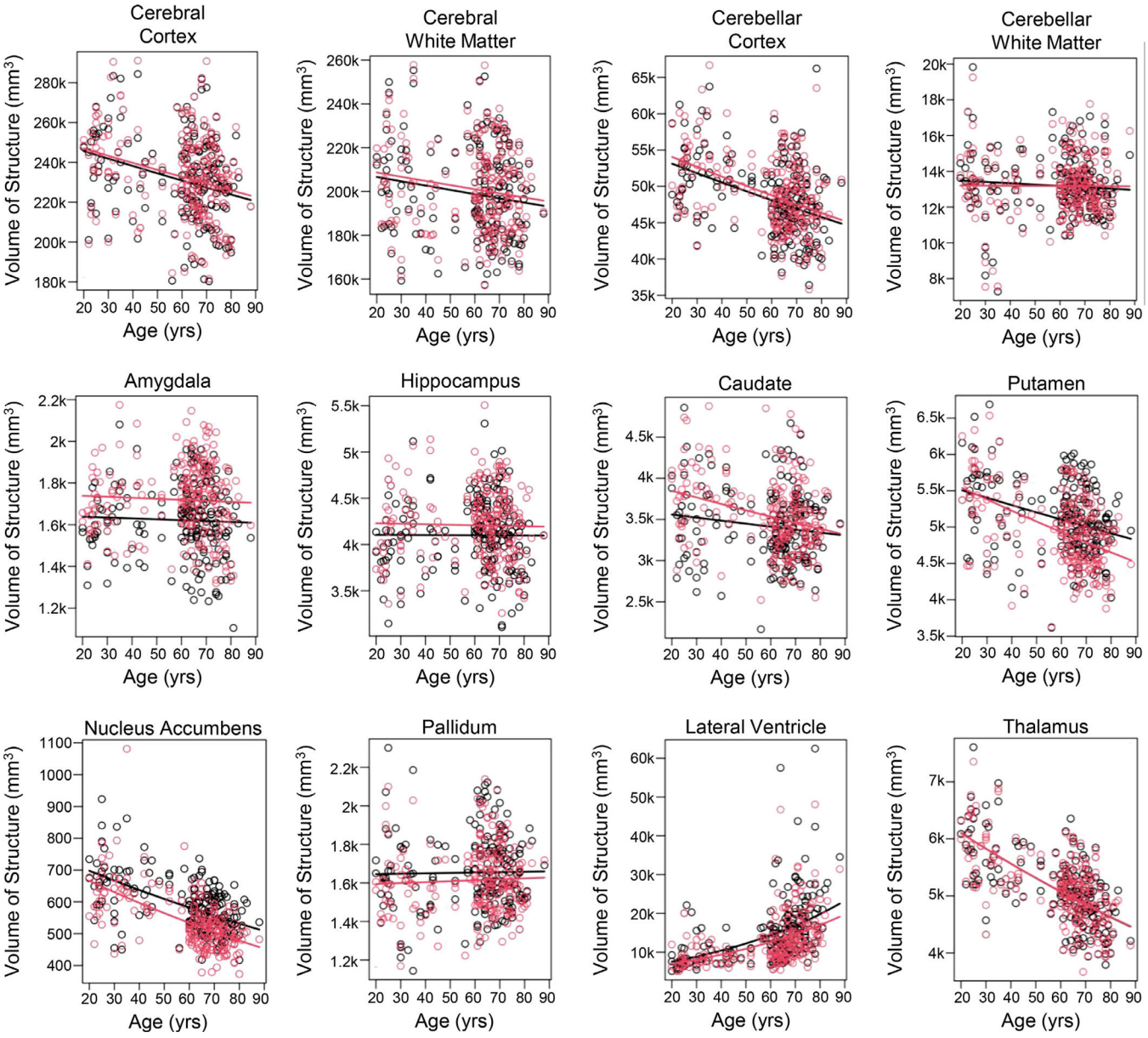


**Fig. 3.**

Absolute volumes of the whole thalamus and extra-thalamic structures plotted versus age. Curves show best fits to the defined exponential regression model. Red=right hemisphere. Black=left hemisphere.

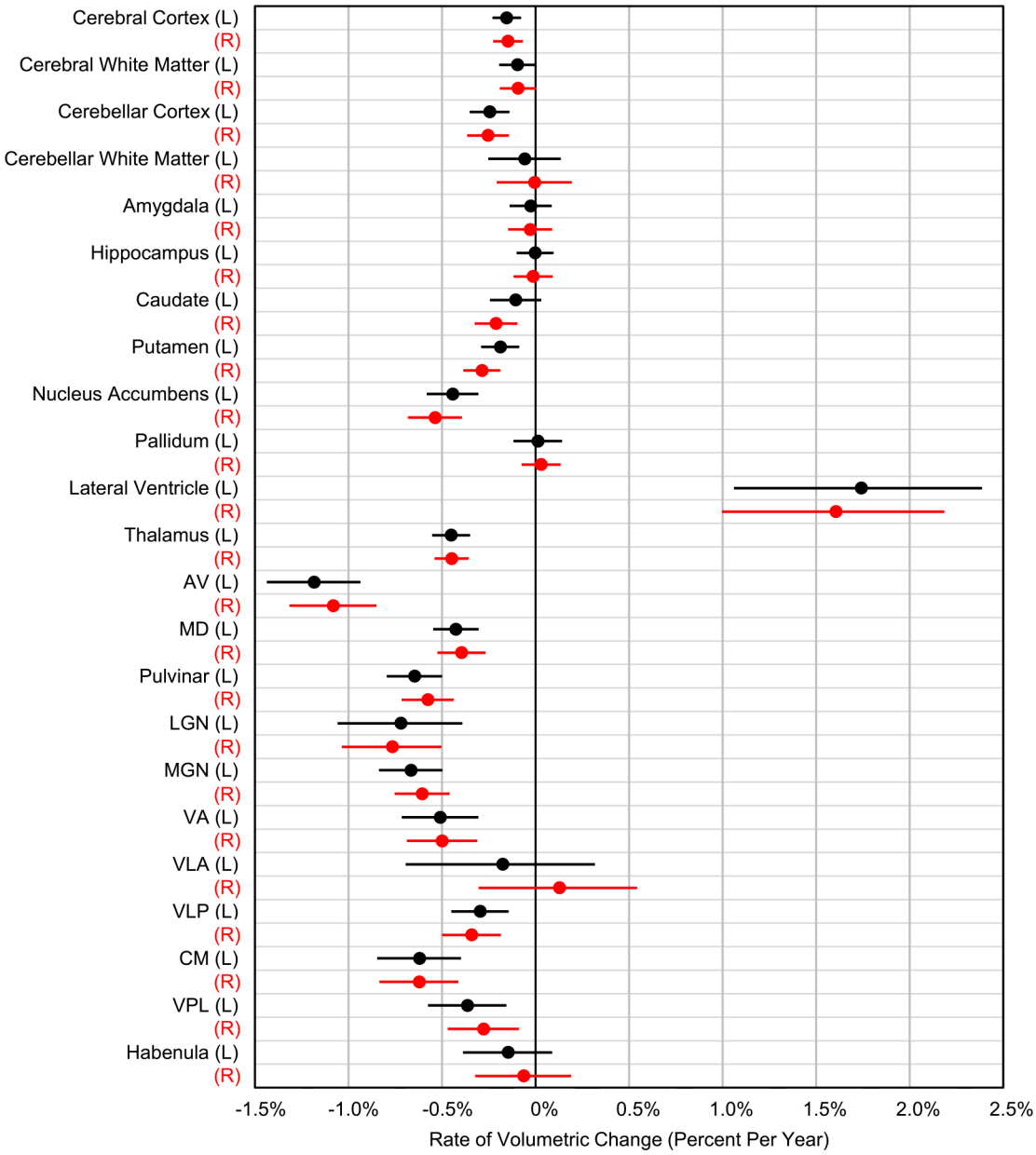


**Fig. 4.**

Comparison of annualized atrophy rates of extra-thalamic and thalamic structures. Lines indicate 95% confidence bands, adjusted for multiple comparisons. Note that thalamic nuclei atrophy at rates higher than most other structures in the brain. Red=right hemisphere. Black=left hemisphere.

**Table 1**

Participant demographics.

| | Bordeaux Younger Participants (< 60 years of age) | Stanford Younger Participants (<60 years of age) | Stanford Older Participants (>=60 years of age) | All Participants |
|---|---|---|---|---|
| Number of Participants | 38 | 17 | 143 | 198 |
| Sex (male, female) | 11 M, 27 F | 9 M, 8 F | 66 M, 77 F | 86 M, 112 F |
| Age (mean / standard deviation/range / range) (yrs) | 33.1 / 10.4 / 20–56 | 37 / 11.4 / 24–58 | 69.1 / 6.1 / 60–88 | 59.4 / 17.4 / 20–88 |
| Education Level (mean / standard deviation / range) (yrs) | 21 / 0 / 21–21 | 20.2 / 1.8 / 16–21 | 16.7 / 2.0 / 10–20 | 17.8 / 2.6 / 10–21 |

**Table 2**

Image acquisition parameters.

| | Bordeaux Younger Subjects | | | | Stanford Younger Subjects | | Stanford Older Subjects | |
|---|---|---|---|---|---|---|---|---|
| | Tl-weighted Protocol 1 | Tl-weighted Protocol 2 | WMnMPRAGE Protocol 1 | WMnMPRAGE Protocol 2 | Tl-weighted | WMnMPRAGE | Tl-weighted | WMnMPRAGE |
| Number of Subjects | 22 | 16 | 22 | 16 | 17 | 17 | 143 | 143 |
| Scanner | GE MR750 | Canon Galan | GE MR750 | Canon Galan | GE MR750 | GE MR950 | GE MR750 | GE MR950 |
| Field Strength | 3T | 3T | 3T | 3T | 3T | 7T | 3T | 7T |
| Head Coil | 32 channel (GE Healthcare) | 32 channel (Canon) | 32 channel (GE Healthcare) | 32 channel (Canon) | 32 channel (Nova Medical) | 32 channel (Nova Medical) | 32 channel (Nova Medical) | 32 channel (Nova Medical) |
| Base Sequence | 3D BRAVO | 3D MPRAGE | 3D MPRAGE | 3D MPRAGE | 3D MPRAGE | 3D MPRAGE | 3D BRAVO | 3D MPRAGE |
| Voxel Size (mm) | 1.0 × 1.0 × 1.0 | 0.6 × 0.6 × 0.6 | 1.0 × 1.0 × 1.0 | 0.8 × 0.8 × 0.8 | 0.8 × 0.8 × 0.8 | 1.0 × 1.0 × 1.0 | 0.9 × 0.9 × 0.9 | 1.0 × 1.0 × 1.0 |
| TE (ms) | 3.2 | 3 | 4.7 | 3.6 | 3.9 | 4.6 | 2.8 | 4.6 |
| TR (ms) | 8.5 | 7 | 11.1 | 7.8 | 8.5 | 10.1 | 7.3 | 10.1 |
| TI (ms) | 400 | 950 | 500 | 470 | 1200 | 680 | 450 | 680 |
| TS (ms) | – | – | 4500 | – | 3700 | 5500 | – | 5500 |
| Flip Angle (degrees) | 11 | 9 | 7 | 7 | 6 | 4 | 12 | 4 |
| Receive Bandwidth (kHz) | +/− 31.25 | +/− 51.3 | +/− 11.9 | +/− 53.4 | +/− 19.2 | +/− 11.9 | +/− 41.67 | +/− 11.9 |
| Slice Number | 180 | 234 | 220 | 200 | 250 | 220 | 186 | 220 |
| Views Per Segment | – | – | 240 | 240 | – | 240 | – | 240 |
| Acceleration Factor | – | 1.5 | 1.25×1.25 | 1.5 | 3 | 3 | 1.75 | 3 |
| Slice Orientation | sagittal | sagittal | coronal | axial | coronal | coronal | sagittal | coronal |
| Scan Time (min) | 10 | 4.5 | 7.2 | 11.2 | 4 | 11.1 | 4.8 | 11.1 |

**Table 3**

Annualized atrophy rates (percent change in volume per year) of thalamic and extra-thalamic structures with 95% confidence bounds and p-values adjusted for multiple comparisons. Bold numbers indicate change that is significantly different from zero.

| Hemisphere | Structure | Mean Volumetric Change Per Year | 95% Confidence Bound-Lower Limit | 95% Confidence Bound-Upper Limit | Adjusted P-Value |
|---|---|---|---|---|---|
| **Left** | **Cerebral Cortex** | **−0.15%** | **−0.23%** | **−0.08%** | **<0.001** |
| Left | Cerebral White Matter | −0.10% | −0.19% | 0.00% | 0.052 |
| **Left** | **Cerebellar Cortex** | **−0.24%** | **−0.35%** | **−0.14%** | **<0.001** |
| Left | Cerebellar White Matter | −0.06% | −0.25% | 0.14% | 1 |
| Left | Amygdala | −0.03% | −0.14% | 0.09% | 1 |
| Left | Hippocampus | 0.00% | −0.10% | 0.10% | 1 |
| Left | Caudate | −0.11% | −0.24% | 0.03% | 0.31 |
| **Left** | **Putamen** | **−0.19%** | **−0.29%** | **−0.09%** | **<0.001** |
| **Left** | **Nucleus Accumbens** | **−0.44%** | **−0.58%** | **−0.30%** | **<0.001** |
| Left | Pallidum | 0.01% | −0.12% | 0.14% | 1 |
| **Left** | **Lateral Ventricle** | **1.74%** | **1.10%** | **2.42%** | **<0.001** |
| **Left** | **Thalamus** | **−0.45%** | **−0.55%** | **−0.35%** | **<0.001** |
| **Left** | **AV** | **−1.18%** | **−1.43%** | **−0.93%** | **<0.001** |
| **Left** | **MD** | **−0.43%** | **−0.55%** | **−0.30%** | **<0.001** |
| **Left** | **Pulvinar** | **−0.65%** | **−0.79%** | **−0.50%** | **<0.001** |
| **Left** | **LGN** | **−0.72%** | **−1.05%** | **−0.38%** | **<0.001** |
| **Left** | **MGN** | **−0.67%** | **−0.83%** | **−0.50%** | **<0.001** |
| **Left** | **VA** | **−0.51%** | **−0.71%** | **−0.30%** | **<0.001** |
| Left | VLA | −0.18% | −0.67% | 0.34% | 0.999 |
| **Left** | **VLP** | **−0.30%** | **−0.45%** | **−0.14%** | **<0.001** |
| **Left** | **CM** | **−0.62%** | **−0.84%** | **−0.39%** | **<0.001** |
| **Left** | **VPL** | **−0.36%** | **−0.57%** | **−0.15%** | **<0.001** |
| Left | Habenula | −0.15% | −0.38% | 0.10% | 0.704 |
| **Right** | **Cerebral Cortex** | **−0.15%** | **−0.23%** | **−0.07%** | **<0.001** |
| Right | Cerebral White Matter | −0.09% | −0.19% | 0.00% | 0.075 |
| **Right** | **Cerebellar Cortex** | **−0.25%** | **−0.36%** | **−0.14%** | **<0.001** |
| Right | Cerebellar White Matter | 0.00% | −0.20% | 0.20% | 1 |

| Hemisphere | Structure | Mean Volumetric Change Per Year | 95% Confidence Bound-Lower Limit | 95% Confidence Bound-Upper Limit | Adjusted P-Value |
|---|---|---|---|---|---|
| Right | Amygdala | −0.03% | −0.15% | 0.09% | 1 |
| Right | Hippocampus | −0.01% | −0.12% | 0.09% | 1 |
| **Right** | **Caudate** | **−0.21%** | **−0.32%** | **−0.10%** | **<0.001** |
| **Right** | **Putamen** | **−0.29%** | **−0.38%** | **−0.19%** | **<0.001** |
| **Right** | **Nucleus Accumbens** | **−0.54%** | **−0.68%** | **−0.39%** | **<0.001** |
| Right | Pallidum | 0.03% | −0.07% | 0.14% | 1 |
| **Right** | **Lateral Ventricle** | **1.61%** | **1.03%** | **2.22%** | **<0.001** |
| **Right** | **Thalamus** | **−0.45%** | **−0.54%** | **−0.36%** | **<0.001** |
| **Right** | **AV** | **−1.08%** | **−1.31%** | **−0.84%** | **<0.001** |
| **Right** | **MD** | **−0.40%** | **−0.52%** | **−0.27%** | **<0.001** |
| **Right** | **Pulvinar** | **−0.58%** | **−0.71%** | **−0.43%** | **<0.001** |
| **Right** | **LGN** | **−0.77%** | **−1.03%** | **−0.49%** | **<0.001** |
| **Right** | **MGN** | **−0.61%** | **−0.75%** | **−0.46%** | **<0.001** |
| **Right** | **VA** | **−0.50%** | **−0.69%** | **−0.31%** | **<0.001** |
| Right | VLA | 0.13% | −0.29% | 0.56% | 0.999 |
| **Right** | **VLP** | **−0.34%** | **−0.50%** | **−0.18%** | **<0.001** |
| **Right** | **CM** | **−0.62%** | **−0.83%** | **−0.41%** | **<0.001** |
| **Right** | **VPL** | **−0.28%** | **−0.47%** | **−0.09%** | **<0.001** |
| Right | Habenula | −0.06% | −0.32% | 0.20% | 1 |

**Table 4**

Annualized atrophy rates of thalamic nuclei grouped by function. Group atrophy rates were tested with t-tests for significant difference from zero. 95% confidence bands and p-values were adjusted for multiple comparisons. Nuclei are color-coded by functional group: yellow = cognitive; green = visual; pink = auditory/vestibular; blue = motor; and purple = somatosensory.

| Group | Function | Annualized Atrophy Rate | 95% Confidence Bound-Lower Limit | 95% Confidence Bound-Upper Limit | Adjusted P-Value |
|---|---|---|---|---|---|
| AV, MD | Cognitive | 0.53% | 0.62% | 0.44% | <0.001 |
| LGN, Pulvinar | Visual | 0.62% | 0.73% | 0.51% | <0.001 |
| MGN | Auditory/Vestibular | 0.64% | 0.75% | 0.52% | <0.001 |
| VA, VLA, VLP, CM | Motor | 0.37% | 0.48% | 0.26% | <0.001 |
| VPL | Somatosensory | 0.32% | 0.46% | 0.18% | <0.001 |

**Table 5**

Functional specificity in the atrophy of thalamic nuclei with age. Significant between-group differences in atrophy rates were tested with paired t-tests. P-values were adjusted for multiple comparisons. Bold numbers indicate statistical significance.

| Between Group Comparison | Adjusted P-Value |
|---|---|
| Cognitive > Visual | **0.039** |
| **Cognitive > Auditory/Vestibular** | **0.026** |
| **Cognitive > Motor** | **<0.001** |
| **Cognitive > Somatosensory** | **0.006** |
| Visual > Auditory/Vestibular | 0.998 |
| **Visual > Motor** | **<0.001** |
| **Visual > Somatosensory** | **<0.001** |
| **Auditory/Vestibular > Motor** | **<0.001** |
| **Auditory/Vestibular > Somatosensory** | **<0.001** |
| Motor > Somatosensory | 0.929 |